A radiomics nomogram for preoperative prediction of microvascular invasion risk in hepatitis B virus-related hepatocellular carcinoma

Jie Peng ⓘ
Jing Zhang ⓘ
Qifan Zhang ⓘ
Yikai Xu ⓘ
Jie Zhou ⓘ
Li Liu ⓘ

PURPOSE
We aimed to develop and validate a radiomics nomogram for preoperative prediction of microvascular invasion (MVI) in hepatitis B virus (HBV)-related hepatocellular carcinoma (HCC).

METHODS
A total of 304 eligible patients with HCC were randomly divided into training (n=184) and independent validation (n=120) cohorts. Portal venous and arterial phase computed tomography data of the HCCs were collected to extract radiomic features. Using the least absolute shrinkage and selection operator algorithm, the training set was processed to reduce data dimensions, feature selection, and construction of a radiomics signature. Then, a prediction model including the radiomics signature, radiologic features, and alpha-fetoprotein (AFP) level, as presented in a radiomics nomogram, was developed using multivariable logistic regression analysis. The radiomics nomogram was analyzed based on its discrimination ability, calibration, and clinical usefulness. Internal cohort data were validated using the radiomics nomogram.

RESULTS
The radiomics signature was significantly associated with MVI status ($P < 0.001$, both cohorts). Predictors, including the radiomics signature, nonsmooth tumor margin, hypoattenuating halos, internal arteries, and alpha-fetoprotein level were reserved in the individualized prediction nomogram. The model exhibited good calibration and discrimination in the training and validation cohorts (C-index [95% confidence interval]: 0.846 [0.787–0.905] and 0.844 [0.774–0.915], respectively). Its clinical usefulness was confirmed using a decision curve analysis.

CONCLUSION
The radiomics nomogram, as a noninvasive preoperative prediction method, shows a favorable predictive accuracy for MVI status in patients with HBV-related HCC.

From the Hepatology Unit and Department of Infectious Diseases (J.P., L.L. ✉ liuli.fimmu@gmail.com), Department of Medical Imaging Center (J.Z., Y.X.), and Hepatobiliary Surgery (Q.Z., J.Zhou) Nanfang Hospital, Southern Medical University, Guangzhou, China.

Hepatocellular carcinoma (HCC) is the sixth most common type of cancer and ranks third as a cause of cancer-related death globally. Worldwide, approximately 630 000 new cases of HCC occur annually, with more than half of these cases occurring in China (1). This disease is related to hepatitis B virus (HBV) infection in almost 70%–90% of cases in the highly endemic Asia-Pacific regions, especially in China (2, 3). Partial hepatectomy and liver transplantation are the most effective curative treatments, albeit in a limited number of cases (4). Indeed, the 5-year recurrence rates after surgical treatment and liver transplantation are as high as 70% and 35%, respectively (5–7). It is, therefore, necessary to find effective biomarkers that can identify aggressive behavior and predict tumor recurrence after liver resection and transplantation.

In HCC, the presence of microvascular invasion (MVI) is a histopathologic feature indicative of aggressive behavior (8). Previous studies have identified MVI as a major risk factor for early recurrence in the first two years after liver resection and transplantation (9). Precise identification of MVI involvement in patients with HCC is critical to develop treatment strategies and arrive at prognoses. Over the past decade, researchers have made persistent endeavors towards the preoperative prediction of MVI (10–12). Although several radiologic features on contrast-enhanced magnetic resonance imaging (MRI) and computed tomography (CT) images (such as tumor margin, internal arteries, and hypodense halos) are known

to be predictors of MVI status, there is still debate about the best predictive feature of MVI in HCC (13–15). Therefore, establishing these radiologic features require further validation studies. Moreover, there remains a lack of a satisfactory prediction method in HBV-related HCC, and a new method for improving the predictive power of MVI should also be considered (16).

In this regard, radiomics—a quantitative high-throughput extraction method used for converting medical images into high-dimensional extractable data—has attracted increasing attention in recent years (17, 18). Data analysis subsequent to radiomics can aid the decision-making process. Previous reports have indicated that radiomics features could potentially be used as predictive or prognostic biomarkers (19–21). Although a radiomics signature based on CT textural features has been reported as a biomarker for the preoperative prediction of early recurrence in patients with HCC (22), to the best of our knowledge, no study to date has proposed that presence of MVI can be accurately predicted based on a radiomics signature.

Therefore, our study aimed to construct and validate a novel radiomics model, including a radiomics signature, radiologic features, and clinical risk factors, to predict preoperative MVI status in patients with HBV-related HCC.

Methods

Patient selection

This retrospective study was approved by our institutional review board and ethical committee (NFEC-201208-K3). Informed consent forms were signed by all patients. A total of 918 cases of HCC were identified from electronic medical records. The inclusion criteria were as follows: (a) partial hepatectomy with tumor tissues pathologically confirmed to be HCC; (b) validation of clinical data; (c) validation of triphasic

Main points

- We present a radiomics nomogram for predicting presurgical microvascular invasion in HBV-related hepatocellular carcinoma.

- The nomogram exhibits favorable calibration and discrimination for prediction of microvascular invasion.

- It is useful for noninvasively identifying patients with hepatocellular carcinoma with a high microvascular invasion risk.

dynamic CT images acquired within 7 days prior to treatment; and (d) the presence of a single tumor. Exclusion criteria were as follows: (a) history of locoregional therapy (radiofrequency ablation) or liver transplantation; (b) presence of other malignant liver tumors; and (c) presence of two or more tumors. Based on these criteria, 304 patients were finally selected for this study. They were randomly assigned to the training (n=184) or validation (n=120) cohorts. The presence of MVI was confirmed by two pathologists. All patients were enrolled between January 2006 and November 2015.

Baseline clinicopathologic data (age, sex, hepatocirrhosis status, Child–Pugh classification, and alpha-fetoprotein [AFP] level) were gathered from medical records. Serum AFP levels were measured within a week before surgery. In accordance with the normal range used at our center, the threshold value of serum AFP level was 20 ng/mL.

CT image acquisition

Contrast-enhanced CT images were acquired at our hospital using either a SOMATOM (Siemens Medical Systems) and Brilliance iCT 256 (Philips Healthcare) multi-detector row CT (MDCT) scanner. Scanning parameters used in this study were as follows: tube voltage, 120 kVp; detector collimation, 64×0.6 and 128×0.625 mm; field of view, 250–400 mm; pixel size, 512×512; rotation time, 0.5 s; slice interval, 0 mm; slice thickness, 5 mm; and reconstructed section thicknesses, 1 mm. Contrast-enhanced CT images were acquired after the injection of 1.0 mL/kg contrast material (Ultravist 370, Bayer Schering Pharma) into the antecubital vein at a rate of 2.0–3.0 mL/s using a power injector (Ulrich CT Plus 150, Ulrich Medical), followed by a saline flush (20 mL). Triphasic (hepatic arterial, portal venous, and delayed phase) CT images were acquired at 30, 60, and 120 s after contrast material injection. The slice thickness of the reconstructed arterial and portal venous phase images was 5 mm.

Analysis of radiologic features

Preoperative CT images were retrospectively assessed using a Picture Archiving and Communication System with an optimal window setting in each case. Image analysis was performed by two abdominal radiologists (readers 1 and 2, with 11 and 20 years of experience in liver CT imaging, respectively) who were blinded to information on clinical, laboratory, pathologic, and

MVI status. Each image was validated by a senior radiologist. Imaging features were determined for each HCC, in accordance with previous studies (13, 15).

The imaging features were as follows: (a) tumor margin, categorized as a smooth margin when observed to enclose nodular tumors with smooth contours or as a non-smooth margin when observed to enclose non-nodular tumors with an irregular margin with budding portions at the periphery in both hepatic arterial and portal venous images; (b) peritumoral enhancement, which was defined by the presence of a detectable region of enhancement adjacent to the tumor border in the arterial phase, which later exhibited attenuation compared with the background liver parenchyma on CT images in the equilibrium phase; (c) a hypoattenuating halo, which was defined as a rim of hypoattenuation partially or completely circumscribing the tumor on peritumoral portal venous images; (d) internal arteries, which were defined by the persistence of discrete arterial enhancement within the tumor in the arterial phase; and (e) a tumor–liver difference, which was defined as a focal or circumferential sharp transition of attenuation between the tumor and adjacent liver parenchyma in arterial phase images.

Segmentation of regions of interest and extraction of radiomic features

Regions of interest (ROIs) in tumors were semi-automatically segmented in the largest cross-sectional area using the IBEX software package (open source, source-code version), which was developed in 64-bit MATLAB 2014b (Math Works). Tumor ROIs were manually segmented by an abdominal radiologist with 11 years of experience; a senior radiologist with 20 years of experience confirmed each ROI.

In this study, 980 candidate radiomics features were generated from each patient, 490 features each from arterial and portal venous phase images. Each image was prepared by using a Gaussian smooth filter (size=3, sigma=0.5) to decrease noise. All feature extraction methods employed IBEX software using in-house developed texture analysis algorithms. The 980 extracted features included the following key features: intensity direct, intensity histogram, gray-level run-length matrix (GLRLM), gray-level co-occurrence matrix (GLCM), neighbor intensity difference, and shape.

Selection of MVI-status-related features and construction of a radiomics signature

A logistical model was built using the least absolute shrinkage and selection operator (LASSO) algorithm. The λ with the smallest cross-validation error was chosen. Finally, eight features were selected, and a formula for the radiomics score (rad-score) was generated using a linear combination of the chosen features weighted by the LASSO method. A radiomics signature was developed using the rad-scores. The Mann-Whitney U test was used to evaluate potential relationships between the radiomics signature and MVI status in the training and validation cohorts.

Construction and validation of the radiomics nomogram

The radiomics signature, nonsmooth tumor margin, internal arteries, hypoattenuating halos, and AFP level were tested in a multivariate logistic regression model for prediction of MVI in the training cohort. In this way, a radiomics nomogram was constructed and used as a quantitative tool for predicting MVI status in the training cohort.

The internal validation cohort was evaluated using the radiomics nomogram, and the total points for each patient were calculated and then evaluated as a predictive factor for MVI. Finally, the C-index and calibration curve were generated from the regression model. Using Harrell's C-index, the discrimination capability of the radiomics model in the training cohort was quantitated. Bootstrapping validation (1000 bootstrap resamples) was performed to calculate a relatively corrected C-index in the validation cohort.

Clinical utility

For evaluating the clinical utility of the nomogram, the probabilities of net benefits were quantified at different thresholds in the combined training and validation cohorts by decision curve analysis (DCA).

Statistical analysis

The LASSO logistic regression model was applied with penalty parameter tuning, which was achieved by 10-fold cross-validation. A likelihood ratio test with backward step-down selection was applied to the multivariate logistic regression model. All statistical tests were performed using the R statistical software version 3.3.3. The "glmnet" package was used for executing the LASSO algorithm. Receiver operating characteristic (ROC) curves were plotted using the "pROC" package. The nomogram and calibration plots were constructed using the "rms" package, while DCA was performed using the "dca.R" package. Chi-square test and Mann-Whitney U test were analyzed by R statistical software. Two-sided P values <0.05 were considered significant.

Results

The patient recruitment process and study flowchart are presented in Supplemental Figs. S1 and S2, respectively. The development process of the radiomics model is presented in Fig. 1. The baseline clinical characteristics of the training and validation cohorts are listed in Table 1. There was no significant difference in prevalence of MVI between the two cohorts ($P = 0.185$); the MVI positivity rates were 69% and 61.7% in the training and validation cohorts, respectively. There were no significant differences in other clinical characteristics between the two cohorts (Table S1).

This study employed axial CT images for analysis of radiologic features (Supplemental Fig. S3). A significant difference was observed in the prevalence of nonsmooth tumor margins between MVI-positive and MVI-negative patients in the training cohort ($P = 0.015$); this difference was later confirmed in the validation cohort as well ($P = 0.008$; Table 1). We found arterial peritumoral enhancement had no significant difference in training and validation cohorts ($P = 0.301$ and $P = 0.556$, respectively; Table 1). Hypoattenuating halos and internal arteries showed significant differences between MVI-positive and MVI-negative patients in both cohorts (Table 1). Tumor–liver difference was observed and there was no significant difference between MVI-positive and MVI-negative patients in either cohort ($P = 0.994$ and $P = 0.888$, respectively).

A total of 980 features were extracted from CT images (490 each from hepatic arterial and portal venous phase images; Fig. 2a). Eight features (five and three features, respectively, from hepatic arterial and portal venous phase images) that were significantly related to MVI status in the training cohort were chosen for construction of the radiomics signature (Fig. 2b). In both cohorts, MVI-positive patients exhibited higher rad-scores than MVI-negative patients ($P < 0.001$, both).

The results of multivariate logistic regression analysis demonstrated that the radiomics signature, AFP level, internal ar-
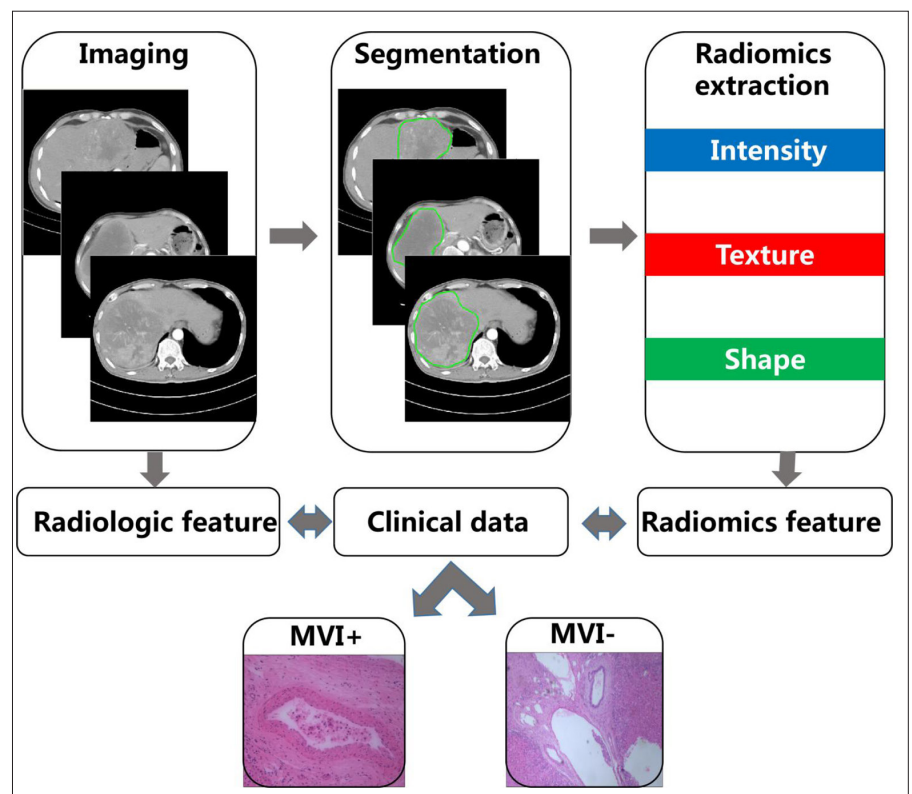

Figure 1. Flowchart of the model development process in this study.

Table 1. Characteristics of patients in the training and validation cohorts

Characteristic	Training cohort			Validation cohort		
	MVI present	MVI absent	P	MVI present	MVI absent	P
Age (yrs), median (range)	53 (21–77)	52 (15–79)	0.291	55 (24–73)	47 (19–73)	0.025*
Sex			0.657			0.084
Male	108 (58.7)	47 (25.5)		61 (50.8)	43 (35.8)	
Female	19 (10.3)	10 (5.4)		13 (10.8)	3 (2.5)	
HBsAg status			0.189			0.572
Positive	96 (52.2)	48 (26.1)		61 (50.8)	36 (30.0)	
Negative	31 (16.9)	9 (4.9)		13 (10.8)	10 (8.3)	
Child-Pugh classification			0.765			0.166
A	107 (58.1)	49 (26.6)		63 (52.5)	43 (35.8)	
B	20 (10.9)	8 (4.3)		11 (9.2)	3 (2.5)	
AFP (ng/mL)			<0.001*			< 0.001*
≤20	30 (16.3)	31 (16.9)		17 (14.2)	25 (20.8)	
>20	97 (52.7)	26 (14.1)		57 (47.5)	21 (17.5)	
Hepatocirrhosis status			0.004*			0.894
Present	65 (35.3)	42 (22.8)		49 (40.8)	31 (25.8)	
Absent	62 (33.7)	15 (8.1)		25 (20.8)	15 (12.5)	
Tumor size (cm), median (range)	6.30 (1.00–20.00)	5.70 (1.8–19.5)	0.498	6.35 (0.80–15.20)	4.90 (0.30–17.20)	0.453
Nonsmooth tumor margin			0.015*			0.008*
Present	82 (44.6)	26 (14.1)		53 (44.2)	22 (18.3)	
Absent	45 (24.5)	31 (16.9)		21 (17.5)	24 (20.0)	
Arterial peritumoral enhancement			0.301			0.556
Present	17 (9.2)	11 (6)		14 (11.7)	7 (5.8)	
Absent	110 (59.8)	46 (25.0)		64 (53.3)	43 (35.8)	
Hypoattenuating halos			0.014*			0.008*
Present	29 (15.8)	23 (12.5)		13 (10.8)	18 (15.0)	
Absent	98 (53.3)	34 (18.5)		61 (50.8)	28 (23.3)	
Internal arteries			0.001*			< 0.001*
Present	79 (42.9)	21 (11.4)		46 (38.3)	13 (10.8)	
Absent	48 (26.1)	36 (19.6)		28 (23.3)	33 (27.5)	
Tumor–liver difference			0.994			0.888
Present	20 (10.9)	9 (4.9)		7 (5.8)	4 (3.3)	
Absent	107 (58.1)	48 (26.1)		67 (55.8)	42 (35.0)	
Radiomics score, median (range)	1.676 (-2.076 to 5.626)	-0.012 (-4.453 to 3.114)	< 0.001*	1.127 (-1.450 to 5.331)	-0.041 (-4.099 to 2.537)	< 0.001*

Data are presented as n (%) unless otherwise noted. *P* values are derived from univariable association analysis between each of the clinicopathologic variables and MVI status.
HBsAg, Hepatitis B surface antigen; AFP, alpha-fetoprotein; MVI, microvascular invasion.
*P < 0.05 indicates statistical significance.

teries, and nonsmooth tumor margin were independent predictors of MVI (Table 2). Notably, hypoattenuating halo was also an important predictor of MVI (Tables 1 and 2). Therefore, a radiomics nomogram was constructed with radiomics signature, AFP level, hypoattenuating halos, arterial per- itumoral enhancement, and nonsmooth tumor margin status as predictors of MVI (Fig. 3). In the training cohort, this model showed a favorable C-index of 0.846 (95% confidence interval [CI], 0.787–0.905) and good calibration upon bootstrapping vali- dation (Table 2).

The radiomics nomogram presented a similar C-index (0.844; 95% CI, 0.774– 0.915) in the validation set. The calibration curves demonstrated good consistency between the nomogram-estimated and actual fre- quencies of MVI (Fig. 4). On the basis of the maximum Youden index, the optimal cutoff

Table 2. Risk factors for microvascular invasion in hepatocellular carcinoma

		Model	
Intercept and variables	β	Odds ratio (95% CI)	P
Intercept	-1.372		0.006*
Radiomics signature	0.771	5.252 (2.811–9.813)	<0.001*
Nonsmooth tumor margin	1.127	3.088 (1.383–6.895)	0.005*
Internal arteries	1.104	3.017 (1.382–6.584)	0.005*
Hypoattenuating halos	-0.722	0.485 (0.210–1.117)	0.089
AFP level	0.857	2.358 (1.038–5.358)	0.04*
C-index			
Training cohort		0.846 (0.787–0.905)	
Validation cohort		0.844 (0.774–0.915)	

β, regression coefficient; AFP, alpha-fetoprotein.
*$P < 0.05$ indicates statistical significance.
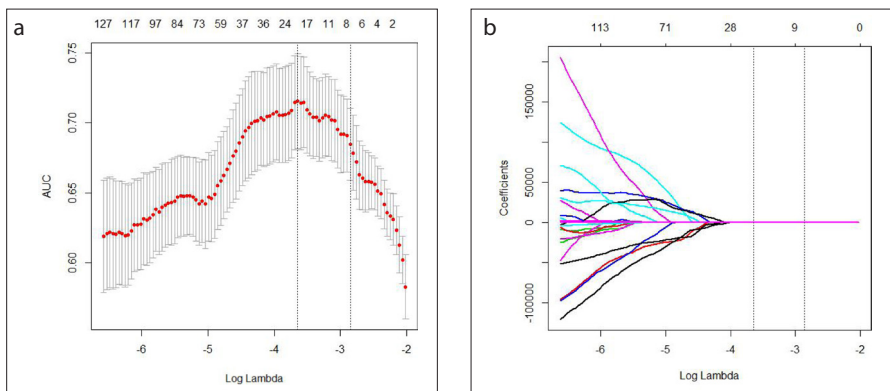
Figure 2. a, b. Selection of radiomics features using the LASSO logistic regression model. Panel **(a)** shows LASSO coefficient analysis of the 980 radiomics features. Using 10-fold cross-validation, the minimum value of log (λ) was found to be -2.855 based on the 1-SE criteria. Panel **(b)** shows coefficients plotted against the log (λ) sequence. Eight nonzero coefficients (indicated by a vertical line in the plot) were selected.
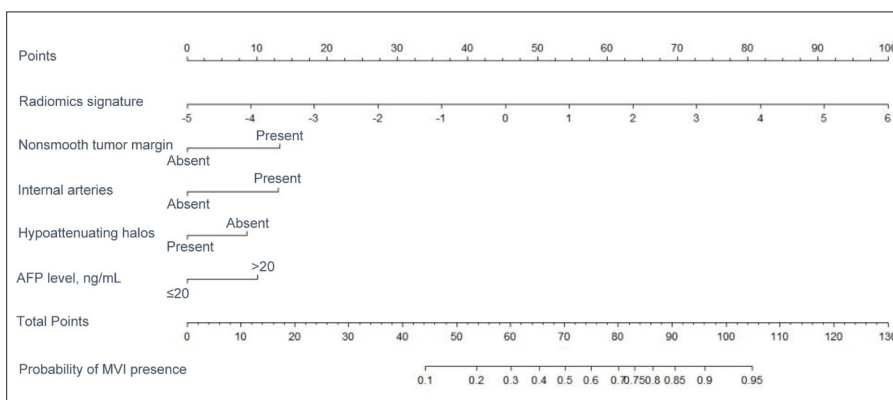
Figure 3. Construction of the radiomics nomogram. In the training set, the radiomics nomogram incorporated radiomics signature, nonsmooth tumor margin, internal arteries, hypoattenuating halos, and AFP levels.

value of all nomogram scores in the training set was defined to be 60. The sensitivity and specificity of the radiomics nomogram were 79.53% (95%CI, 71.46–86.17%) and 71.93% (95%CI, 58.46–83.03%) in the training cohort and 75.68% (95%CI, 64.31–84.90) and 80.43% (95%CI, 66.09–90.64%) in the validation cohort, respectively (Table S2).

According to the results of DCA of the radiomics nomogram (Fig. 5), when the threshold probability is ~10% or 30%, the radiomics nomogram and radiomics signatures will provide a greater benefit than the "treat-all" or "treat-none" strategies. The threshold probability is ~46%–88% in radiologic features that integrate AFP levels and the radiomics signature showed a better ability to discriminate the MVI compared with radiologic features. By combining the radiomics signature and radiologic features, this radiomics nomogram exhibited a greater overall net benefit than the radiomics signature and radiologic features, including AFP levels. Moreover, the area under the ROC curve of the radiomics nomogram was significantly higher than the radiomics signature or radiologic features that included AFP levels ($P = 0.023$ and $P = 0.008$, respectively).

Discussion

In the present study, which involved patients with HCC (approximately 80% related to HBV infection), we developed a nomogram that included CT-based radiomics features, radiologic features, and clinical data as a new method for individualized prediction of MVI before therapy in HBV-related HCC. To our knowledge, this is the first study to employ radiomics for evaluation of MVI in HCC. We confirmed capability of the radiomics model for preoperative individualized prediction of MVI status in a validation cohort.

Recent studies have demonstrated that radiomics signatures could be used to determine the risk of lymph-node metastasis in patients with colorectal and bladder cancer (23, 24). Radiomics signatures have been reported to be important pretreatment prognostic predictors for progression-free and overall survival in patients with cancer (25–28). Similarly, in the present study, a radiomics signature involving multiple radiomics features was demonstrated to be significantly associated with MVI status. We developed a nomogram that integrated radiomics signature with radiologic features and AFP level to further improve its predictive accuracy for MVI. The radiomics nomogram exhibited a good C-index value in the training and validation cohorts. Therefore, with the added advantage of noninvasiveness, this CT-image-derived radiomics model can be used as a convenient biomarker for prediction of MVI status.
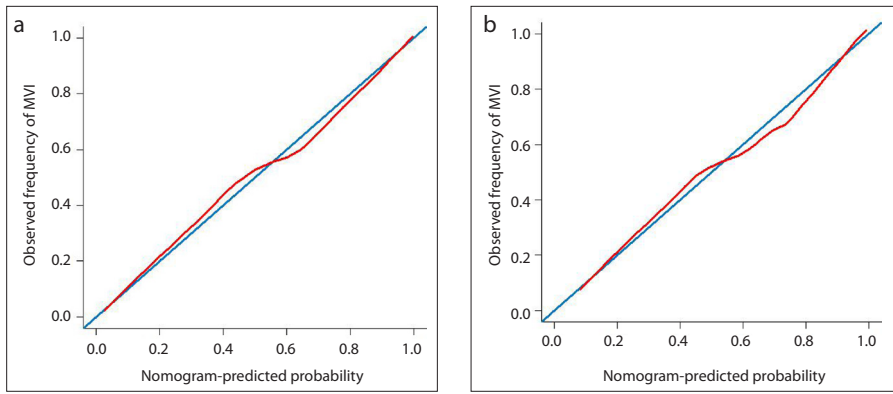
Figure 4. a, b. Calibration curves of radiomics nomogram-based prediction in the training and validation cohorts. To validate the predictive ability of the nomogram, calibration curves in the training (**a**) and validation (**b**) groups were analyzed. The calibration curves represent the calibration of the nomogram based on agreement between the predicted risk of MVI and actual MVI findings. A closer fit between the red and blue lines indicates better predictive accuracy of the nomogram.
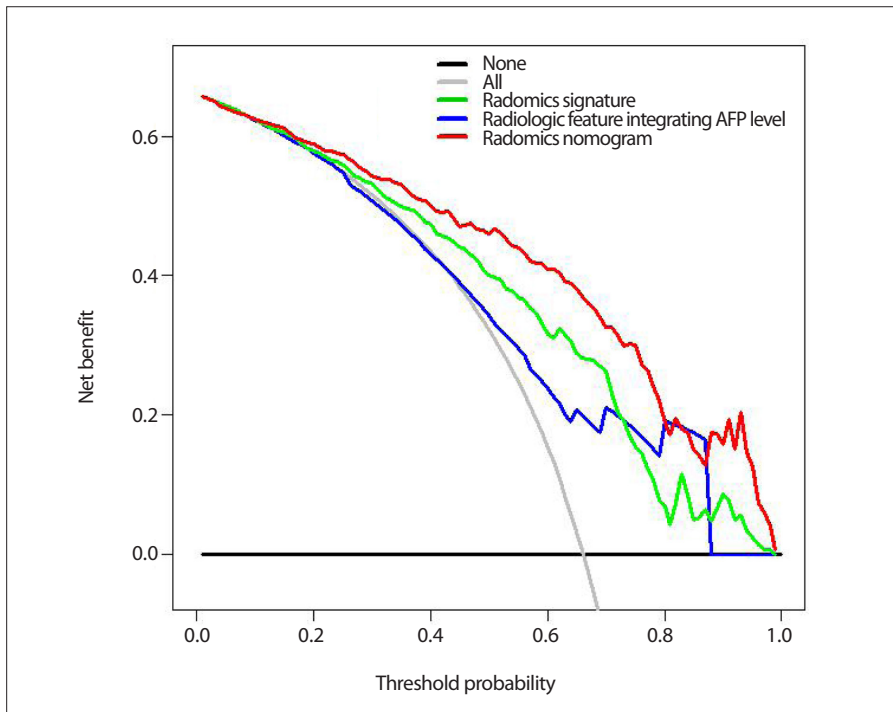
Figure 5. Findings of DCA for the entire cohort (n=304). The decision curve indicates that when the threshold probability of a patient was ~10%, use of the radiomics nomogram for predicting MVI would provide greater benefit than the "treat-all" patients or "treat-none" schemes. The curve of the radiomics nomogram over the radiomics signature and radiologic features that integrated AFP levels showed the greatest benefit.

In the present study, presence of non-smooth tumor margins, hypoattenuating halos, and internal arteries was significantly associated with MVI status in the training and validation cohorts, which is in agreement with the results of previous studies (29–32). A previous study reported radiogenomic venous invasion (RVI), which included internal arteries, hypodense halo, and tumor–liver difference, as a contrast-enhanced CT biomarker for prediction of MVI (13). Another study reported "two-trait predictor of venous invasion" (TTPVI), which included internal arteries and hypodense halo, to exhibit a high predictive accuracy (15). However, these previous studies were limited by the irrelatively small sample sizes and lack of internal or external validation. In the present study, in addition to the radiomics nomogram, we also validated RVI and TTPVI and discovered that our radiomics nomogram exhibited a higher accuracy for prediction of MVI in the combined training and validation cohorts (Supplemental Fig. S4). This indicates that our nomogram could be more suitable than the previous two biomarkers for prediction of MVI in HBV-related HCC.

In previous studies, multifocal lesions, large tumor size, advanced neoplasm grade, and high serum AFP level have been reported to increase the possibility of vascular invasion in advanced HCC (33–35). In the present study, abnormal AFP level, an independent risk factor for MVI, was also significantly associated with MVI. However, tumor size and neoplasm grade were not associated with MVI status in either cohort in our study; this finding is in agreement with that of Chandarana et al. (36) and inconsistent with that of Renzulli et al. (15). There are conflicting data regarding the efficiency of tumor size in predicting MVI in HCC. These discrepancies are probably because of selection bias; in the present study, nearly 66% of patients with HCC exhibited MVI positivity, with a mean tumor size of 6.7 cm.

The most important and final goal of a nomogram is the imperative to explain individual requirements for additional treatment (37). We determined the sensitivity and specificity of our nomogram for predicting the risk of MVI, using 60 as the cutoff value. Patients with scores ≥60 had a greater risk of MVI relative to the rest. We also evaluated the radiomics nomogram of all patients by DCA and calculated the net benefit by summing up the benefits and subtracting the ill effects, weighting the latter by a factor associated with the relative harm of undetected cancer to that of unnecessary treatment (38). This new approach provides insights into the clinical consequences of threshold probabilities as well as information regarding the net benefit. The decision curve indicated that, when the threshold probability was 10%, use of the radiomics model for prediction of MVI provided a greater benefit than the overall-treatment or no-treatment strategies. Thus, our nomogram can serve as a non-invasive preoperative predictive tool for assessment of MVI status in patients with HBV-related HCC.

This study has some limitations. It should be mentioned that our study lacked external validation for the model and requires further multicenter validation with a larger sample size to obtain more convincing evidence in favor of clinical application of the radiomics nomogram. Additionally, ap-

plication of a combination of gene markers (a 91-gene "venous-invasion marker panel" derived from gene-expression analysis of HCC tumors with histologically confirmed MVI) and the radiomics signature might improve the efficiency of MVI prediction in patients with HCC (39).

In conclusion, we developed a noninvasive radiomics nomogram (including a radiomics signature, radiologic features, and clinical risk factors) that exhibited favorable accuracy for preoperative individualized prediction of MVI status in HBV-related HCC. Multicenter retrospective validation and prospective randomized clinical trials are needed to obtain stronger evidence in favor of clinical application of our radiomics nomogram.

Conflict of interest disclosure

The authors declared no conflicts of interest.

References

1. Ding J, Wang H. Multiple interactive factors in hepatocarcinogenesis. Cancer Lett 2014; 346:17–23. [CrossRef]
2. El-Serag HB. Epidemiology of viral hepatitis and hepatocellular carcinoma. Gastroenterology 2012; 142:1264–1273. [CrossRef]
3. Yuen MF, Hou JL, Chutaputti A, Asia Pacific Working Party on Prevention of Hepatocellular C. Hepatocellular carcinoma in the Asia pacific region. J Gastroen Hepatol 2009; 24:346–353. [CrossRef]
4. Lei Z, Li J, Wu D, et al. Nomogram for Preoperative Estimation of Microvascular Invasion Risk in Hepatitis B Virus-Related Hepatocellular Carcinoma Within the Milan Criteria. JAMA Surg 2016; 151:356–363. [CrossRef]
5. Fong Y, Sun RL, Jarnagin W, Blumgart LH. An analysis of 412 cases of hepatocellular carcinoma at a Western center. Ann Surg 1999; 229:790–799. [CrossRef]
6. Grazi GL, Ercolani G, Pierangeli F, et al. Improved results of liver resection for hepatocellular carcinoma on cirrhosis give the procedure added value. Ann Surg 2001; 234:71–78. [CrossRef]
7. Lim KC, Chow PK, Allen JC, et al. Microvascular invasion is a better predictor of tumor recurrence and overall survival following surgical resection for hepatocellular carcinoma compared to the Milan criteria. Ann Surg 2011; 254:108–113. [CrossRef]
8. Bruix J, Llovet JM. Hepatitis B virus and hepatocellular carcinoma. J Hepatol 2003; 39 Suppl 1:S59–63. [CrossRef]
9. Renzulli M, Buonfiglioli F, Conti F, et al. Imaging features of microvascular invasion in hepatocellular carcinoma developed after direct-acting antiviral therapy in HCV-related cirrhosis. Eur Radiol 2018; 28:506–513. [CrossRef]

10. Kim MJ, Lee M, Choi JY, Park YN. Imaging features of small hepatocellular carcinomas with microvascular invasion on gadoxetic acid-enhanced MR imaging. Eur J Radiol 2012; 81:2507–2512. [CrossRef]
11. Rodriguez-Peralvarez M, Luong TV, Andreana L, Meyer T, Dhillon AP, Burroughs AK. A systematic review of microvascular invasion in hepatocellular carcinoma: diagnostic and prognostic variability. Ann Surg Oncol 2013; 20:325–339. [CrossRef]
12. Witjes CD, Willemssen FE, Verheij J, et al. Histological differentiation grade and microvascular invasion of hepatocellular carcinoma predicted by dynamic contrast-enhanced MRI. J Mag Res Imag 2012; 36:641–647. [CrossRef]
13. Banerjee S, Wang DS, Kim HJ, et al. A computed tomography radiogenomic biomarker predicts microvascular invasion and clinical outcomes in hepatocellular carcinoma. Hepatology 2015; 62:792–800. [CrossRef]
14. Lee S, Kim SH, Lee JE, Sinn DH, Park CK. Preoperative gadoxetic acid-enhanced MRI for predicting microvascular invasion in patients with single hepatocellular carcinoma. J Hepatol 2017; 67:526–534. [CrossRef]
15. Renzulli M, Brocchi S, Cucchetti A, et al. Can Current Preoperative Imaging Be Used to Detect Microvascular Invasion of Hepatocellular Carcinoma? Radiology 2016; 279:432–442. [CrossRef]
16. Unal E, Idilman IS, Akata D, Ozmen MN, Karcaaltincaba M. Microvascular invasion in hepatocellular carcinoma. Diagn Interv Radiol 2016; 22:125–132. [CrossRef]
17. Aerts HJ, Velazquez ER, Leijenaar RT, et al. Decoding tumour phenotype by noninvasive imaging using a quantitative radiomics approach. Nat Commun 2014; 5:4006. [CrossRef]
18. Gillies RJ, Kinahan PE, Hricak H. Radiomics: Images are more than pictures, they are data. 2016; 278:563–577. [CrossRef]
19. Kuo MD, Gollub J, Sirlin CB, Ooi C, Chen X. Radiogenomic analysis to identify imaging phenotypes associated with drug response gene expression programs in hepatocellular carcinoma. J Vasc Interv Radiol 2007; 18:821–831. [CrossRef]
20. Kuo MD, Jamshidi N. Behind the numbers: Decoding molecular phenotypes with radiogenomics--guiding principles and technical considerations. Radiology 2014; 270:320–325. [CrossRef]
21. Lambin P, Rios-Velazquez E, Leijenaar R, et al. Radiomics: extracting more information from medical images using advanced feature analysis. Eur J Cancer 2012; 48:441–446. [CrossRef]
22. Zhou Y, He L, Huang Y, et al. CT-based radiomics signature: a potential biomarker for preoperative prediction of early recurrence in hepatocellular carcinoma. Ab Radiol 2017; 42:1695–1704. [CrossRef]
23. Huang YQ, Liang CH, He L, et al. Development and Validation of a Radiomics Nomogram for Preoperative Prediction of Lymph Node Metastasis in Colorectal Cancer. J Clin Oncol 2016; 34:2157–2164. [CrossRef]
24. Wu S, Zheng J, Li Y, et al. A Radiomics Nomogram for the Preoperative Prediction of Lymph Node Metastasis in Bladder Cancer. Clin Cancer Res 2017; 23: 6904–6911. [CrossRef]
25. Fu YP, Yi Y, Huang JL, et al. Prognostic Nomograms Stratify Survival of Patients with Hepatocellular Carcinoma Without Portal Vein Tumor Thrombosis After Curative Resection. Oncologist 2017; 22:561–569. [CrossRef]

26. Grossmann P, Narayan V, Chang K, et al. Quantitative Imaging Biomarkers for Risk Stratification of Patients with Recurrent Glioblastoma Treated with Bevacizumab. Neuro-oncology 2017; 19: 1688–1697. [CrossRef]
27. Lao J, Chen Y, Li ZC, et al. A Deep Learning-Based Radiomics Model for Prediction of Survival in Glioblastoma Multiforme. Sci Rep-UK 2017; 7:10353. [CrossRef]
28. Zhang B, Tian J, Dong D, et al. Radiomics Features of Multiparametric MRI as Novel Prognostic Factors in Advanced Nasopharyngeal Carcinoma. Clin Cancer Res 2017; 23:4259–4269. [CrossRef]
29. Cucchetti A, Piscaglia F, Grigioni AD, et al. Preoperative prediction of hepatocellular carcinoma tumour grade and micro-vascular invasion by means of artificial neural network: a pilot study. J Hepatol 2010; 52:880–888. [CrossRef]
30. Kobayashi T, Aikata H, Honda F, et al. Preoperative Fluorine 18 Fluorodeoxyglucose Positron Emission Tomography/Computed Tomography for Prediction of Microvascular Invasion in Small Hepatocellular Carcinoma. J Comput Assist Tomo 2016; 40:524–530. [CrossRef]
31. Wu TH, Hatano E, Yamanaka K, et al. A nonsmooth tumor margin on preoperative imaging predicts microvascular invasion of hepatocellular carcinoma. Surg Today 2016; 46:1275–1281. [CrossRef]
32. Zhao H, Hua Y, Dai T, et al. Development and validation of a novel predictive scoring model for microvascular invasion in patients with hepatocellular carcinoma. Eur J Radiol 2017; 88:32–40. [CrossRef]
33. Fakhry C, Zhang Q, Nguyen-Tan PF, et al. Development and Validation of Nomograms Predictive of Overall and Progression-Free Survival in Patients With Oropharyngeal Cancer. J Clin Oncol 2017; 35:4057–4065. [CrossRef]
34. McHugh PP, Gilbert J, Vera S, Koch A, Ranjan D, Gedaly R. Alpha-fetoprotein and tumour size are associated with microvascular invasion in explanted livers of patients undergoing transplantation with hepatocellular carcinoma. HPB 2010; 12:56–61. [CrossRef]
35. Schlichtemeier SM, Pang TC, Williams NE, et al. A pre-operative clinical model to predict microvascular invasion and long-term outcome after resection of hepatocellular cancer: The Australian experience. Eur J Surg Oncol 2016; 42:1576–1583. [CrossRef]
36. Chandarana H, Robinson E, Hajdu CH, Drozhinin L, Babb JS, Taouli B. Microvascular invasion in hepatocellular carcinoma: is it predictable with pretransplant MRI? AJR Am J Roentgenol 2011; 196:1083–1089. [CrossRef]
37. Wang Y, Li J, Xia Y, et al. Prognostic nomogram for intrahepatic cholangiocarcinoma after partial hepatectomy. J Clin Oncol 2013; 31:1188–1195. [CrossRef]
38. Vickers AJ, Cronin AM, Elkin EB, Gonen M. Extensions to decision curve analysis, a novel method for evaluating diagnostic tests, prediction models and molecular markers. BMC Med Inform Decis 2008; 8:53. [CrossRef]
39. Chen X, Cheung ST, So S, et al. Gene expression patterns in human liver cancers. Mol Bio Cell 2002; 13:1929–1939. [CrossRef]

Radiomics score (Rad-score) calculation formula	
Rad-score =	2.529
	+1.899* $P\_IntensityDirect\_LocalEntropyMean$
	-9.534* $P\_GLRLM\_90ShortRunEmphasis$
	-4.004e-06 * $P\_GLRLM\_0LongRunHighGrayLevelEmpha$
	+2.598* $A\_Shape\_Roundness$
	-3.740e-06 * $A\_GLRLM\_0LongRunHighGrayLevelEmpha$
	-1.715* $A\_GLCM\_0.4InverseVariance$
	-1.218* $A\_GLCM\_135.4Contrast$
	-5.196* $A\_GLCM\_0.1Contrast$
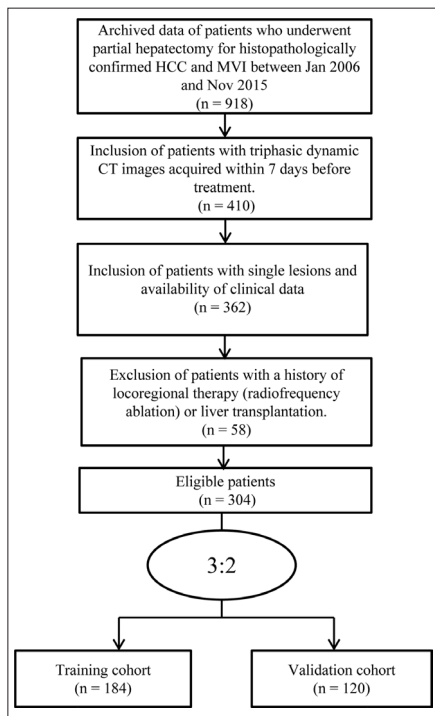
Figure S1. Recruitment pathways for patients with HCC. CT, computed tomography; HCC, hepatocellular carcinoma; MVI, microvascular invasion.

Table S1. Participant characteristics in the training and validation cohorts

| Characteristics	Training cohort (n=184)	Validation cohort (n=120)	P
Age, years, median (range)	53 (15–79)	49 (19–73)	0.170
Sex			
Male	155	104	0.560
Female	29	16	
HBsAg status			0.588
Positive	144	97	
Negative	40	23	
Child–Pugh classification			0.380
A	156	106	
B	28	14	
AFP (ng/mL)			0.739
≤20	61	42	
>20	123	78	
Hepatocirrhosis status			0.135
Present	107	80	
Absent	77	40	
Tumor size (cm), median (range)	6.0 (1.0–20.0)	5.45 (0.3–17.2)	0.061
Nonsmooth tumor margin			0.507
Present	108	75	
Absent	76	45	
Arterial peritumoral enhancement			0.596
Present	28	21	
Absent	156	99	
Hypoattenuating halos			0.382
Present	52	31	
Absent	132	99	
Internal arteries			0.376
Present	100	59	
Absent	84	61	
Tumor–liver difference			0.096
Present	29	11	
Absent	155	109	
Radiomics score, median (range)	1.14 (-4.45 to 5.63)	0.756 (-4.10 to 5.33)	0.055

Data are presented as n unless otherwise noted. P values are derived from univariable association analysis between each of the clinicopathologic variables and MVI status. AFP, alpha-fetoprotein; HBsAg, Hepatitis B surface antigen; MVI, microvascular invasion.*$P < 0.05$ means statistical significance.

Table S2. Accuracy of the prediction score of the nomogram for estimating the risk of microvascular invasion

| Variable	Value (95% confidence interval)	
	Training cohort	Validation cohort
Area under the ROC curve, concordance index	0.846 (0.787–0.905)	0.844 (0.774–0.915)
Cutoff score	60	60
Sensitivity, %	79.53 (71.46–86.17)	75.68 (64.31–84.90)
Specificity, %	71.93 (58.46–83.03)	80.43 (66.09–90.64)
Likelihood ratio	2.83	3.86

ROC, receiver operating characteristic.
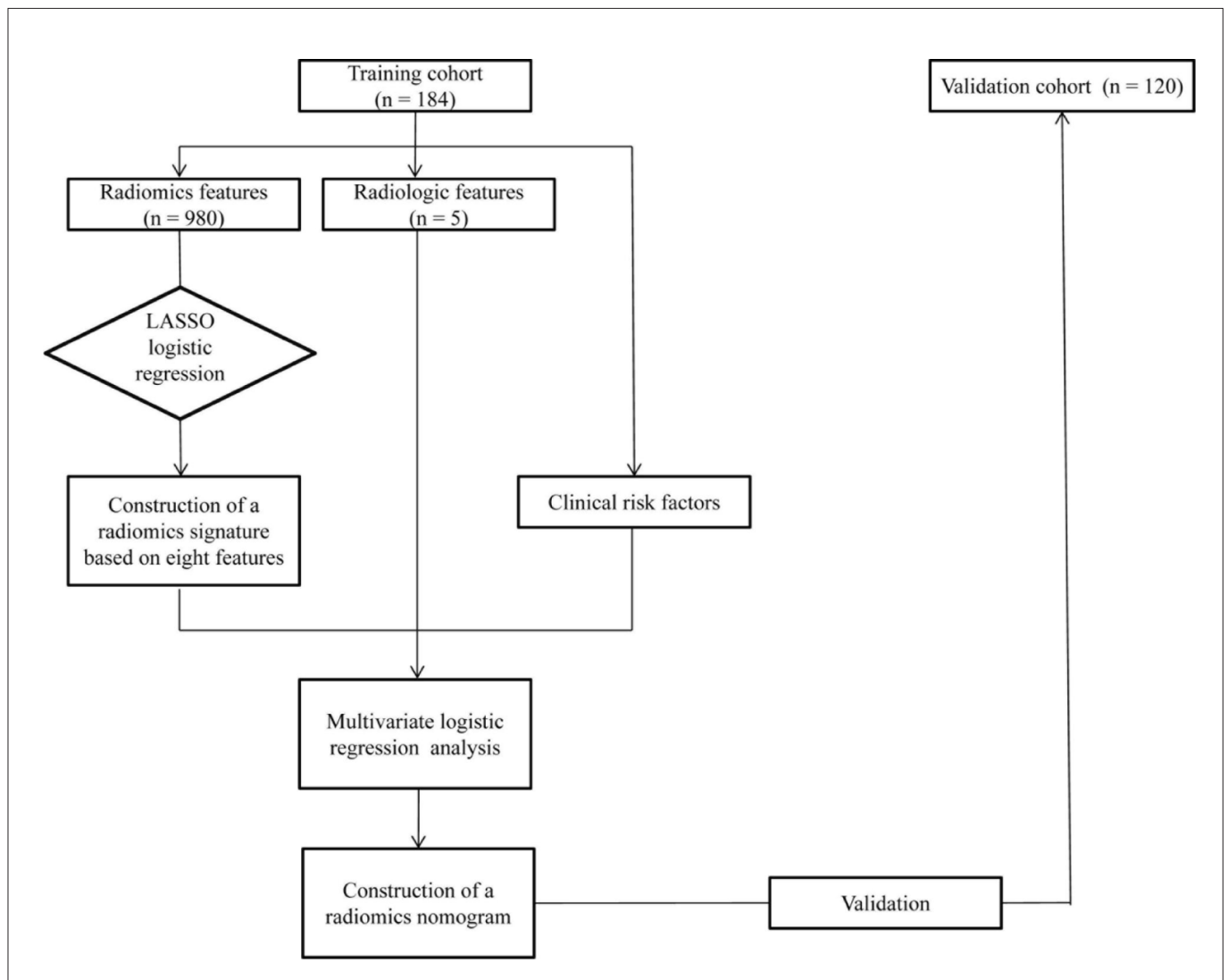
Figure S2. Study flowchart.
LASSO, least absolute shrinkage and selection operator.
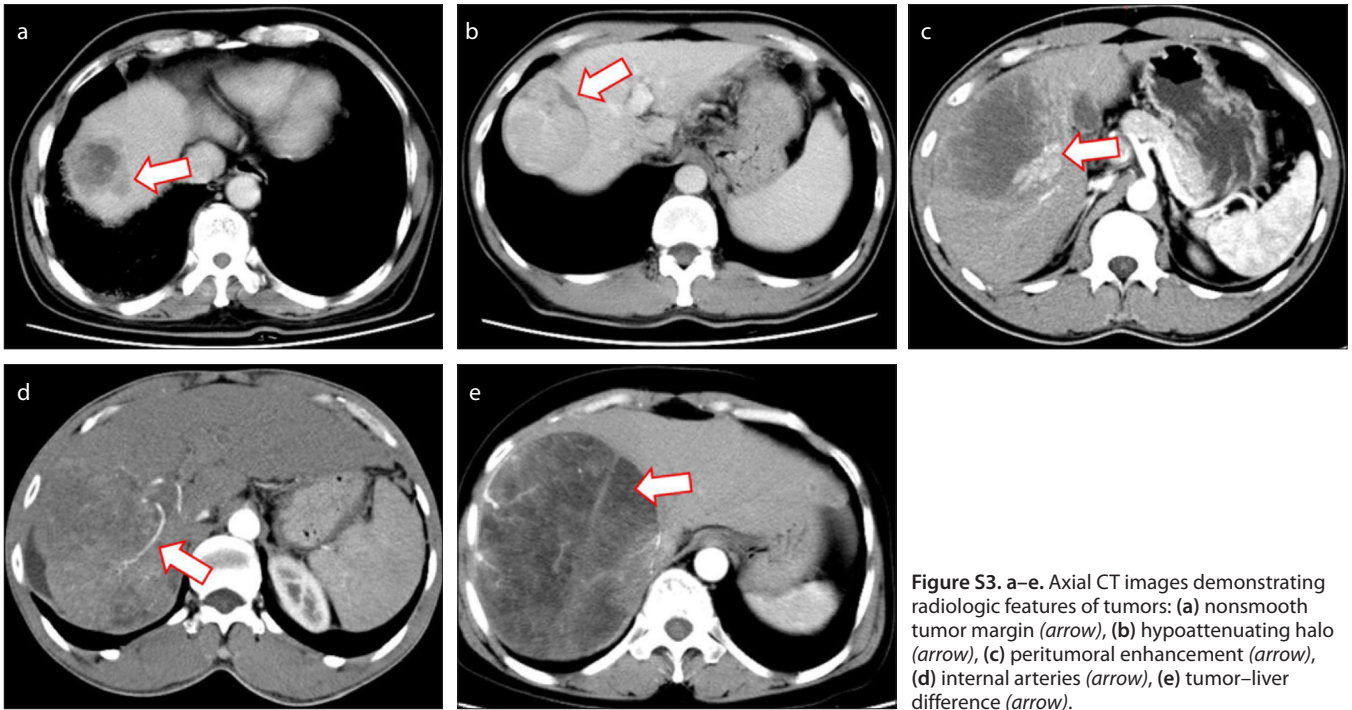
Figure S3. a–e. Axial CT images demonstrating radiologic features of tumors: **(a)** nonsmooth tumor margin *(arrow)*, **(b)** hypoattenuating halo *(arrow)*, **(c)** peritumoral enhancement *(arrow)*, **(d)** internal arteries *(arrow)*, **(e)** tumor–liver difference *(arrow)*.
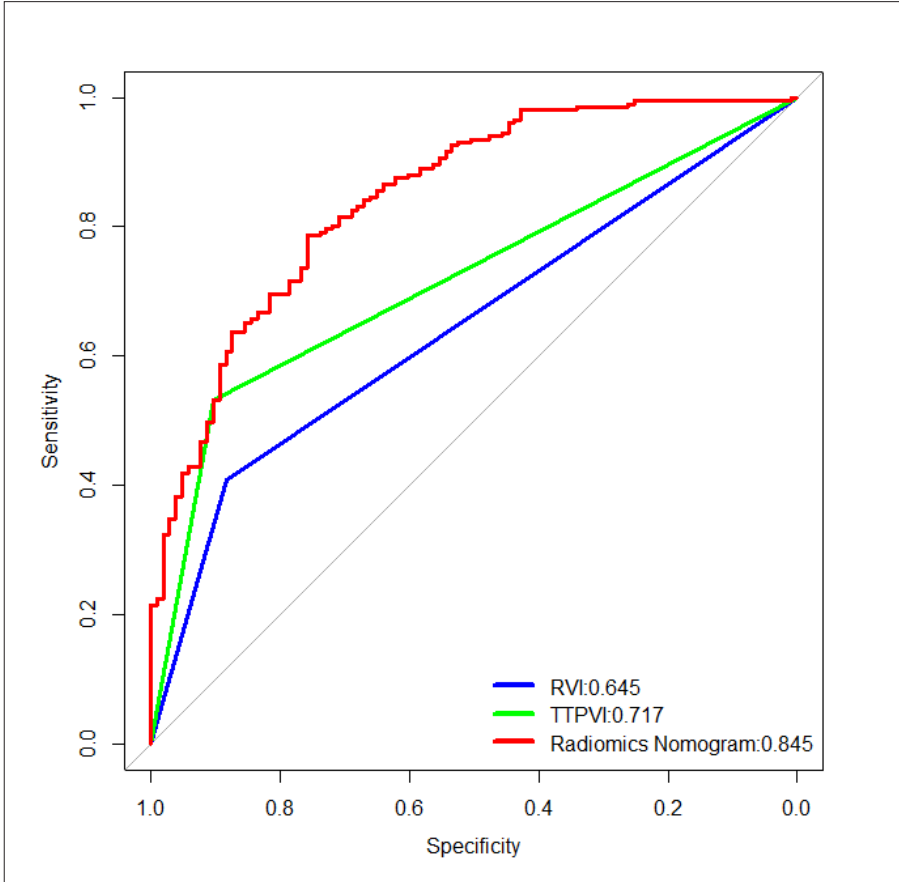
Figure S4. Performance of radiogenomic venous invasion (RVI), two-trait predictor of venous invasion (TTPVI), and the radiomics nomogram in the combined training and validation cohorts (n=304). The results of the bootstrap (n=2000) test for three ROC curves indicated that the AUC of the sum of radiomics nomograms was significantly higher than those of the sole presence of RVI and TTPVI (*P* < 0.001, both). The difference in AUC between TTPVI and RVI was also significant (*P* = 0.027).